International Symposium
On Turbulence and Shear Flow
Phenomena (TSFP-8)
August 28 - 30, 2013 Poitiers, France

PLASMA-BASED MANIPULATION OF SECONDARY FLOW TOWARDS PRESSURE RECOVERY ENHANCEMENT IN A 3D DIFFUSER: A COMPUTATIONAL STUDY

I. Maden, R. Maduta, S. Jakirlić, S. Grundmann and C. Tropea
Department of Mechanical Engineering
Institute of Fluid Mechanics and Aerodynamics (SLA) / Center of Smart Interfaces (CSI)
Technische Universität Darmstadt
Petersenstrasse 17, D-64287 Darmstadt, Germany
maden@csi.tu-darmstadt.de, s.jakirlic@sla.tu-darmstadt.de

J.K. Eaton
Department of Mechanical Engineering, Stanford University
Stanford, CA 94305, USA

ABSTRACT

The present work focusses on the computational study of plasma-actuated flow control towards pressure recovery enhancement with respect to flow reversal weakening in a 3D diffuser configuration, investigated experimentally by Grundmann *et al.* (2011). The measurements were conducted by utilizing a streamwise-oriented arrangement of a dielectric barrier discharge plasma actuator mounted on the top wall of the inflow duct. Herewith a counter-rotating pair of streamwise vortices was generated modifying the inflow towards increase of turbulence intensity. The most efficient scenario, contributing mostly to the pressure recovery implies an actuator configuration pulsed with 40% duty cycle (pertinent to forcing frequency $fmod = 50$ Hz and forcing amplitude corresponding to operating voltage $E_{pl} = 10000 V_{pp}$). The present computational study is primarily concerned with this case assessing it comparatively to the baseline configuration with no actuation imposed. Simulations are performed within the Unsteady RANS (Reynolds-Averaged Navier Stokes) framework by using an eddy-resolving Second-Moment Closure as a subscale model, Maduta and Jakirlić (2011). The plasma actuator was simulated by using a force-distribution database based on the PIV (Particle Image Velocimetry) measurements of the flow induced by a plasma actuator, Kriegseis *et al.* (2013) and Maden *et al.* (2013). The results obtained with respect to the pressure recovery enhancement pertinent to lowering of the backflow intensity due to appropriate turbulence increase show high potential of the present instability-sensitive turbulence model in conjunction with the plasma actuator model.

INTRODUCTION

The presently investigated three-dimensional diffuser configuration has the task to appropriately increase the static pressure by reducing the velocity field magnitude. Furthermore, the flow field evolution is characterized by a certain velocity profile flattening resulting in a nearly steady outlet flow exhibiting an approximately uniform distribution over the cross-section. Cherry *et al.* (2008) and Cherry *et al.* (2009) investigated experimentally a relevant asymmetric flow configuration. The flow discharges from a rectangular inflow duct into a diffuser section whose upper wall and one side wall expand appropriately. The consequence of such an imposed adverse pressure gradient is appearance of a 'truly' three-dimensional separation pattern occupying systematically the entire upper wall. This database is enriched by a recently conducted Direct Numerical Simulation, Ohlsson *et al.* (2010). The 3D diffuser was used as a popular test case for validating turbulence models in the framework of the ERCOFTAC Workshop Series on Refined Turbulence Modeling; see e.g., Jakirlić *et al.* (2010). Computational studies have shown that the computed flow field is extremely sensitive to the secondary flow currents in the inlet duct. Accordingly, this Reynolds-anisotropy induced flow phenomenon is beyond the reach of the anisotropy-blind eddy-viscosity-based turbulence model resulting in a completely wrong flow field topology - the flow separates entirely at the expanding side wall instead at the upper wall.

The influence of appropriate manipulation of the secondary flow by changing the orientation of the secondary vortex structure towards reducing or entirely eliminating the boundary layer separation within the diffuser section and consequently towards pressure increase was the subject of the experimental work of Grundmann *et al.* (2011). Unlike in a number of flow configurations with a plasma actuator acting in a unidirectional manner with respect to the mean flow (with streamwise forcing resulting in a momentum superimposed to the mean flow one, see e.g., Grundmann and Tropea (2009) for the working principle of the plasma-actuated flow control), the plasma actuator arrangement in the present 3D diffuser acts perpendicular (spanwise forcing) to the mean flow through a pair of counter-rotating streamwise vortices affecting directly the secondary motion intensity and consequently the separated flow within

diffuser. The present objective is the computational study of the latter flow configuration focussing on the application of the recently developed instability-sensitive RANS model of turbulence based on a differential, near-wall Reynolds stress model, Maduta and Jakirlić (2011).

DESCRIPTION OF THE 3D DIFFUSER

Fig. 1-upper displays the diffuser geometry illustrating expansion of a fully-developed duct flow (characterized by a Reynolds number $Re_h = 10000$, based on the bulk inflow velocity and duct height) into a diffuser section. This baseline configuration, explored experimentally by Cherry *et al.* (2008), was adopted by Grundmann *et al.* (2011) to investigate sensitivity of the three-dimensional separating flow pattern in a diffuser by manipulating secondary flow in the upstream duct by an appropriate arrangement of the dielectric barrier discharge (DBD) plasma actuator mounted on its upper wall, Fig. 1-lower.

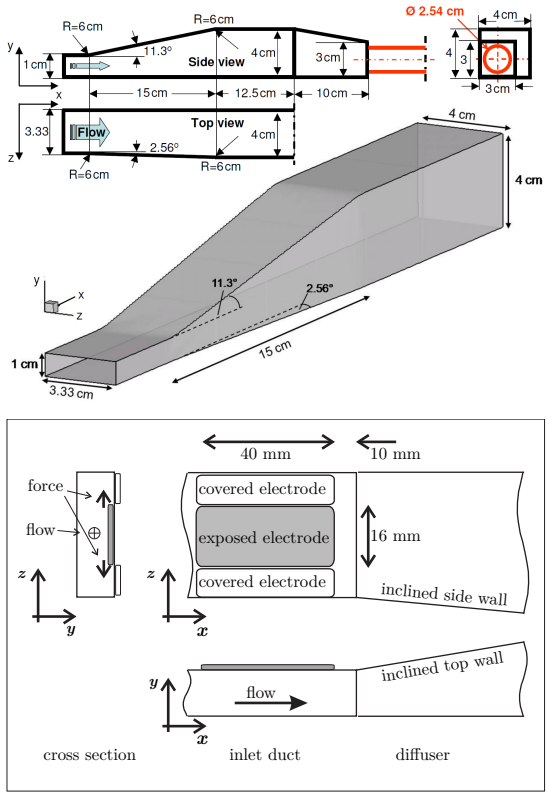

Figure 1. Schematic of the presently investigated 3D diffuser configuration and DBD plasma-actuator arrangement mounted on the top wall of the inflow duct; not in scale. $h = 1\,cm$ represents the inflow duct height.

Grundmann *et al.* (2011) demonstrated that an improvement of the diffuser performance could not be achieved by applying the plasma actuator configuration acting in a unidirectional manner with respect to the mean flow (streamwise forcing). Due to the fact that the diffuser performance exhibits strong sensitivity to the intensity and topology of the secondary vortex structure within the inlet duct Grundmann *et al.* (2011) investigated a completely different actuator arrangement acting perpendicularly to the mean flow (spanwise forcing) direction – through generation of a pair of counter rotating streamwise vortices – causing an appropriate alternation of the orientation of the secondary vortices in the area of the plasma actuator and consequent weakening of the secondary flow intensity in the remaining part of the duct cross-section and the separated flow at the upper diffuser wall. Grundmann *et al.* (2011) investigated performances of two different operating modes of the present plasma-actuator: a continuous mode (Duty Cycle = 100%) and a pulsed mode (DC = 40 %). Fig. 2 displays the experimentally obtained surface pressure distributions at the bottom diffuser wall for all three considered flow configurations: the baseline one and two actuated cases. Whereas the continuously operated plasma actuator deteriorates the diffuser performance reflected by a pressure decrease relative to the baseline configuration the pulsed mode fulfilled the expectation resulting in the pressure recovery enhancement.

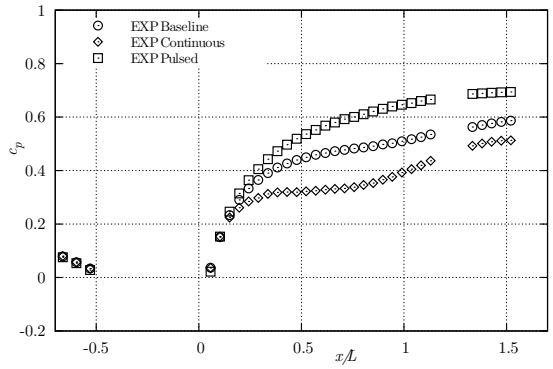

Figure 2. Experimental pressure coefficient distribution at the bottom diffuser wall for the baseline configuration and two actuated flow cases

COMPUTATIONAL METHOD

The unsteady, incompressible, constant fluid property flow in the present 3D diffuser actuated by a dielectric barrier discharge plasma actuator is governed by the following RANS momentum equation:

$$\frac{\partial U_i}{\partial t} + U_j \frac{\partial U_i}{\partial x_j} = -\frac{1}{\rho}\frac{\partial p}{\partial x_i} + \nu \frac{\partial^2 U_i}{\partial x_j \partial x_j} + \frac{\partial}{\partial x_j}\left(-\overline{u_i u_j}\right) + f_i \tag{1}$$

The vector force f_i imparted by the plasma actuator to the fluid flow was presently modeled by applying the force-distribution database extracted directly from the Navier-Stokes equations by feeding them with the velocity field measured by a PIV technique, Kriegseis *et al.* (2013) and Maden *et al.* (2013). Assuming a steady-in-mean, two-dimensional flow with zero-pressure gradient, the imbalance between the convective term and the momentum equation's right-hand-side terms reveals the desired resulting force. This PIV-based volume-force proposal is used presently to model the source term f_i in the above-displayed Reynolds equations closed by a near-wall second-moment closure model formulated in conjunction with the scale-supplying equation governing the homogeneous part of the inverse turbulent time scale ($\omega_h = \varepsilon_h/k$). This turbulent model scheme functions as a sub-scale model in the Unsteady RANS framework. The model capability to account

for the vortex length and time scales variability was enabled through an additional term in the corresponding length-scale determining equation providing a selective assessment of its production, modelled in terms of the von Karman length scale (comprising the second derivative of the velocity field) in line with the SAS (Scale-Adaptive Simulation) proposal (Menter and Egorov (2010)), pertinent particularly to the highly unsteady separated shear layer region. This instability-sensitive Reynolds stress model is capable of obtaining a fluctuating turbulence field also in globally stable flows, such as e.g., attached flow in a plane channel, starting from the steady RANS results. The model proposed does not comprise any parameter depending explicitly on the grid spacing. The model was extensively tested in the past by computing different attached and separated wall-bounded configurations - channel and duct flows, external and internal flows separated from sharp edged and continuous curved surfaces, see Maduta and Jakirlić (2011) for more details. The model results are denoted by IS-RSM throughout the paper. As already discussed the correct capturing of the flow within the diffuser section is strongly correlated with reproduction of the secondary currents induced by the Reynolds stress anisotropy. The incapability of isotropic eddy-viscosity models to reproduce corner vortices makes it necessary to use an anisotropy-resolving model. The adverse pressure gradient causes a complex three-dimensional separation zone (characterized by a non-fixed separation point) starting in the corner built up by two expanding walls. The presently employed Reynolds stress model is capable of capturing such a flow structure.

Numerical method. All computations were performed using the code OpenFOAM, an open source Computational Fluid Dynamics toolbox, utilizing a cell-center-based finite volume method on an unstructured numerical grid and employing the solution procedure based on the PISO procedure for coupling the pressure and velocity fields. The convective transport in momentum equations was discretized with a blending scheme – 95% of the 2nd order central differencing scheme and 5% of the 1st order upwind differencing scheme – implemented in the deferred-correction manner. For the time integration the 2nd order three-point backward scheme was used.

Computational details. The diffuser geometry comprises a part of the inflow duct (length $= 15h$), diffuser section ($L = 15h$) and a reasonably long straight outlet duct (length $= 30h$). The mesh consists of 3.75 Mio. grid cells ($N_x \times N_y \times N_z = 348 \times 91 \times 121$), while $y^+ < 1.5$ has been ensured in the wall-next computational cells. An intensive study performed in the framework of an ERCOFTAC Turbulence Modeling Workshop (see e.g., Jakirlić *et al.* (2010)) led to the presently adopted solution domain (this relates in particular to the outlet duct length) and corresponding grid size. The size of the time step $1 \cdot 10^{-5}\,s$ was chosen to ensure the maximum CFL number < 1. The mean turbulence statistics are collected for a time period of 20 flow-through times; it is recalled that one flow-through time is defined by the ratio of the entire domain length to the bulk velocity at the end of the outlet duct. The inflow planes for the inlet boundary condition are generated by a recycling method (periodic domain $= 10h$ was adopted) as proposed by Baba-Ahmadi and Tabor (2009). The boundary conditions at the outlet plane correspond to a prescribed atmosphere pressure and zero-gradient for all other dependent variables.

RESULTS AND DISCUSSION

The instantaneous streamwise velocity fields displayed in central vertical plane ($z/B = 0.5$) and several streamwise cross-sectional $x-y$ planes in Fig. 3 offer a first impression about the flow in the diffuser for the baseline (upper) and the actuated (DC=40%) configuration (lower). Starting from the steady RANS results in the inflow duct the instability-sensitive model resulted in a highly unsteady turbulent flow field in both diffuser configurations followed by a differently structured separation activity. Based on the recycling method by Baba-Ahmadi and Tabor (2009) the inlet duct is already in structure-resolving mode demonstrating the capability of the proposed model to result in a fluctuating turbulence field also in globally stable flows without imposing any initial fluctuations. The mean axial velocity profile development is displayed in Fig. 4 for the baseline configuration. The present computational results are compared with the experimental and DNS reference displaying a reasonable mutual agreement. The flow reversal pertinent to the upper wall is reasonably predicted. Previously discussed velocity profile flattening whose outcome is an almost uniform profile shape in the outlet duct is obvious.

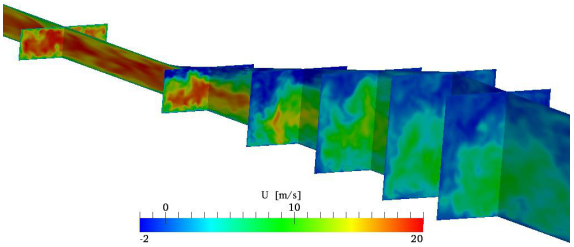

(a) Baseline configuration, IS-RSM

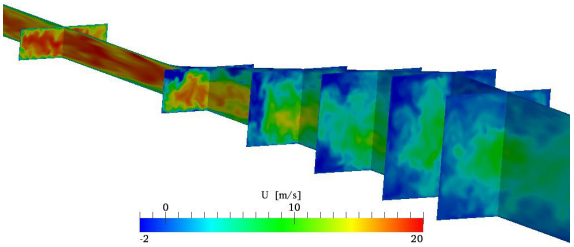

(b) Actuated configuration, IS-RSM

Figure 3. Instantaneous axial velocity contours obtained by IS-RSM model for both considered configurations.

Figs. 5-7 depict the iso-contours of the mean velocity field in the cross-section of the inflow duct corresponding to the very beginning of the duct expansion (at $x/h = 0$) for all three considered diffuser cases illustrating good agreement between experiment and computation. An appropriate narrowing of the cross-sectional area characterized by the maximum velocity value is noticeable in both actuated flow configurations.

The velocity vector plots in Fig. 8 (upper-left) obtained

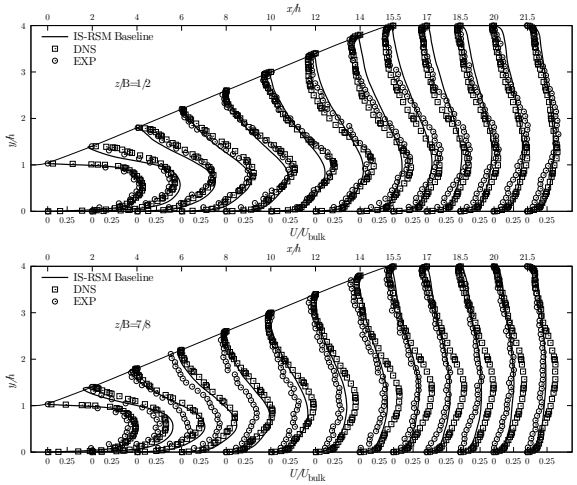

Figure 4. Baseline configuration - streamwise evolution of the mean velocity profiles in the vertical planes at $z/B = 0.5$ (central plane) and $z/B = 0.875$

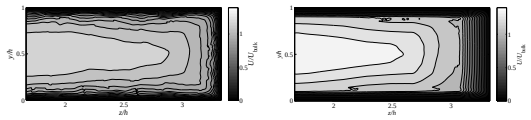

(a) Computation, IS-RSM (b) Experiment

Figure 5. Baseline configuration - time-averaged velocity contours evaluated at the very beginning of the duct expansion (at $x/h = 0$). Only one half of the inflow duct is shown.

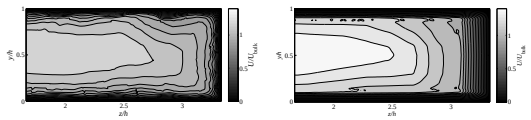

(a) Pulsed mode, IS-RSM (b) Experiment

Figure 6. Time-averaged velocity contours obtained for actuated configuration (pulsed mode) evaluated at the very beginning of the duct expansion (at x/h = 0).

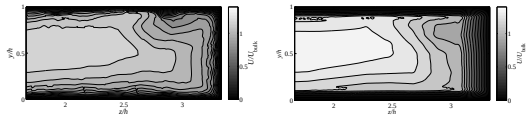

(a) Continuous mode, IS-RSM (b) Experiment

Figure 7. Time-averaged velocity contours obtained for actuated configuration (continuous mode) evaluated at the very beginning of the duct expansion (at x/h = 0).

by the present instability-sensitive IS-RSM model displays a pattern being typical of the secondary motion in a rectangular duct with jets directed to the duct corners and associated vortices at both sides of each jet. As previously discussed this phenomenon is the consequence of the Reynolds stress anisotropy. The forcing imparted by the plasma actuator to the fluid flow into spanwise direction, generating a pair of the streamwise vortices, modifies secondary flow structure towards increase of the turbulence intensity, Fig. 8 (lower-right). The unsteady forcing corresponding to the duty cycle of 40% implies a generation of an oscillating wall jets towards upper duct corners, Fig. 8 (upper-right), characterized by a velocity profile pertinent to an enhanced turbulent level. This oscillatory momentum injection causes an appropriate intensification of the turbulence activity in the boundary layer at upper wall (compared to baseline case, Fig. 8-lower left) transforming into a separated shear layer after discharging into diffuser.

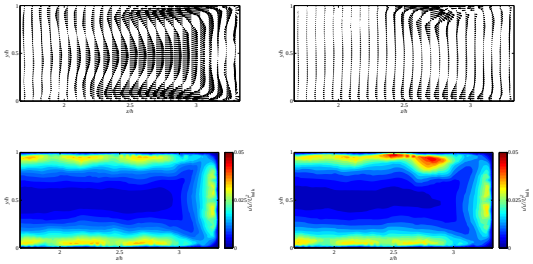

Figure 8. Velocity vectors (upper) and iso-contours of the streamwise Reynolds stress component (lower) in the cross-section of the inflow duct (only one half is shown) obtained by the present instability-sensitive RSM model - (left) baseline configuration with no actuation; (right) actuated configuration with DC=40%.

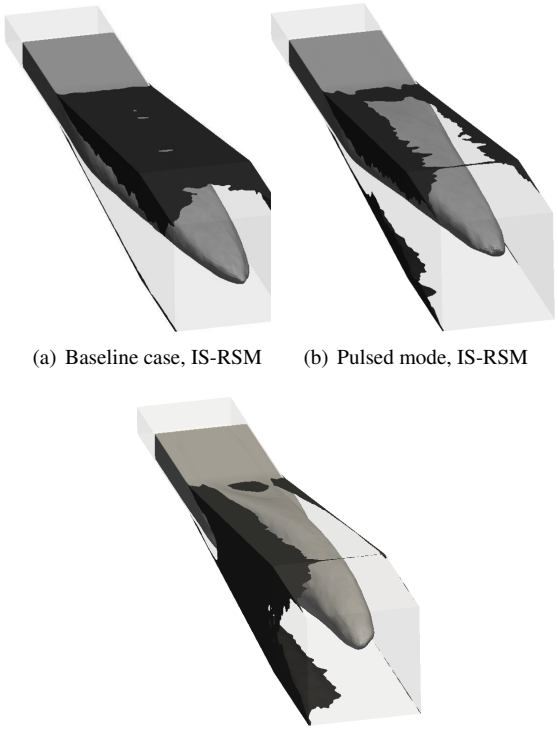

(a) Baseline case, IS-RSM (b) Pulsed mode, IS-RSM

(c) Continuous mode, IS-RSM

Figure 9. Iso-surfaces of axial velocity component $U/U_{\text{bulk}} = -0.01$ and 0.4 for all three diffuser cases.

The modification of the separation process by applying the plasma actuator reflects an appropriate separated

flow topology restructuring relative to the baseline configuration, see Fig. 9. The turbulence intensity in the separated shear layer region is closely correlated with the size of the flow reversal zone - higher turbulence level implies a higher momentum transport across the separated shear layer and consequently shortening or complete elimination of the recirculation bubble. Whereas recirculation bubble occupies the entire upper wall in the diffuser section and consequent straight duct (note black area in the upper-left figure) in the baseline flow, the flow reversal diminishes almost completely in the actuated (pulsed mode) case (upper-right figure). Associated flattening of the velocity field caused by the plasma-actuator is pertinent to a lower velocity maximum. While in the actuated (continuous mode) case the recirculation bubble occupies the entire deflected side wall (lower figure). Grundmann *et al.* (2012) performed an analogous experiment by using differently arranged vortex generators (passive flow control) of a certain dimension (not displayed here) mimicking the effect achieved with the present dielectric barrier discharge plasma actuator with respect to the pressure recovery within the diffuser section. The results obtained by the present model are in a close qualitative agreement with their findings for all three configurations investigated. Figs. 10-12 showing the iso-contours of the axial velocity field in a cross-section corresponding to the outlet straight duct offer a relevant quantitative proof. The zero velocity line (denoted by a thick line) separating the flow reversal zone and the through-flow region exhibits the same shape as the experimentally obtained results. Whereas a tiny separation bubble is found in upper right corner in the baseline configuration and in the lower right corner of the diffuser flow actuated by the continuous mode a through flow characterized by the positive velocity values occupies the cross-sectional area of the outlet duct in its entirety in the diffuser flow actuated by the pulsed mode. The latter finding is pertinent to more symmetric and more flattened velocity profiles taking place even in the initial diffuser part exhibiting no reverse flow corresponding to the pulsed-mode actuated configuration, Fig. 13.

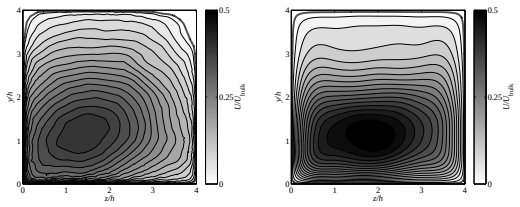

(a) IS-RSM (b) Experiment

Figure 10. Time-averaged velocity contours obtained for baseline configuration at the cross-section located in the straight rear duct at $x/h = 18$.

Figs. 14 show the in-plane velocity vectors in the cross-sectional plane located at $x/h = 15$. For the baseline configuration no clear rotational pattern can be indicated. Whereas a vortex in the actuated configuration is well-marked and located with its centers at $y/h = 0.5$ and $z/h = 3$ indicating a velocity vector field in the upper region corresponding to the more uniform mean flow in the outlet duct.

Figs. 15 illustrate the evolution of the pressure coefficient at the bottom wall of the diffuser section defined as $C_p = (p - p_{ref})/(0.5\rho U_{bulk}^2)$. A more uniform velocity field

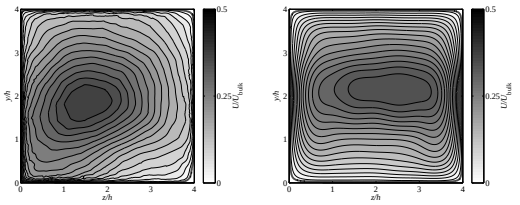

(a) IS-RSM (b) Experiment

Figure 11. Time-averaged velocity contours obtained for actuated (pulsed mode) configuration at the cross-section located in the straight rear duct at $x/h = 18$.

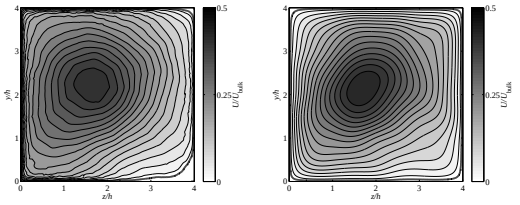

(a) IS-RSM (b) Experiment

Figure 12. Time-averaged velocity contours obtained for actuated (continuous mode) configuration at the cross-section located in the straight rear duct at $x/h = 18$.

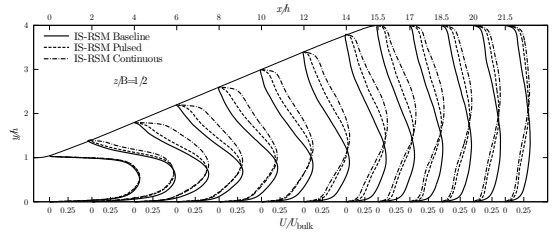

(a) All configurations, $z/B = 0.5$

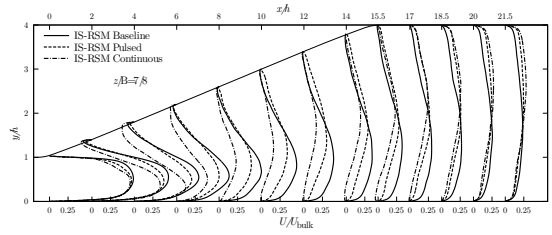

(b) All configurations, $z/B = 0.875$

Figure 13. Streamwise evolution of the computationally obtained axial velocity profiles in two vertical planes at $z/B = 0.5$ (central plane) and at $z/B = 0.875$.

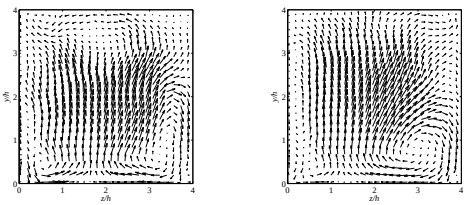

(a) Baseline configuration (b) Pulsed mode

Figure 14. In-plane velocity vectors for both baseline and actuated configurations in a cross-section at $(x/h = 15)$ corresponding to the end of diffuser expansion.

yields consequently an appropriate pressure increase. The pressure recovery enhancement pertinent to the pulsed configuration is obvious compared to the baseline case without flow control. The relevant computationally obtained pressure distributions agree well with reference data. However, this is not the case for the continuously actuated configuration. A tendency towards slight pressure decrease is reproduced computationally but the surface pressure values obtained are somewhat higher compared to the experimental data. Keeping in mind a correctly reproduced separated flow topology within the diffuser section and straight outlet duct (Figs. 9 and 12) it was a non-satisfactory outcome which should be further analyzed.

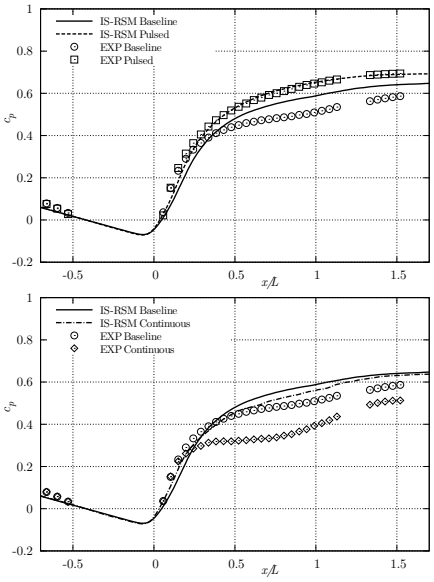

Figure 15. Pressure coefficient distribution at the bottom diffuser wall for baseline and actuated cases.

CONCLUSIONS

Flow in a three-dimensional diffuser whose inflow was appropriately modified by a dielectric barrier discharge plasma actuator aiming at pressure recovery enhancement is investigated computationally by employing an instability-sensitive RANS model of turbulence based on the second-moment level formulation. The restructuring of the separated flow topology reflecting the transformation from a flow reversal zone occupying the entire upper diffuser wall (pertinent to baseline configuration) to the significantly reduced back-flow region, situated mostly in the diffuser corners, and associated velocity profile uniformity could be clearly reproduced. The final outcome corresponding to the pressure increase in the diffuser configuration actuated by a pulsed-mode of the plasma actuator is successfully returned by the computational model. The continuous plasma actuator operating mode simulated computationally ended up with an insufficient pressure decrease compared to the experimental results despite qualitatively correct velocity field.

Acknowledgements. The authors gratefully acknowledge financial support by the German Research Foundation (Deutsche Forschungsgemeinschaft) under grant EXC 259.

REFERENCES

M.H. Baba-Ahmadi, G. Tabor: Inlet conditions for LES using mapping and feedback control. *Computers and Fluids*, Vol. 38(6), pp. 1299-1311, 2009.

E.M. Cherry, C.J. Elkins and J.K. Eaton: Geometric sensitivity of three-dimensional separated flows. *Int. J. Heat and Fluid Flow*, Vol. 29(3), pp. 803-811, 2008.

E.M. Cherry, C.J. Elkins and J.K. Eaton: Pressure measurements in a three-dimensional separated diffuser. *Int. J. Heat and Fluid Flow*, Vol. 30(1), pp. 1-2, 2009.

S. Grundmann and C. Tropea: Experimental Damping of Boundary-Layer Oscillations using DBD Plasma Actuators. *Int. J. Heat and Fluid Flow*, Vol. 30, pp. 394-402, 2009.

S. Grundmann, E.L. Sayles and J.K. Eaton: Sensitivity of an asymmetric 3D diffuser to plasma-actuator induced inlet condition perturbations. *Exp. in Fluids*, Vol 50, pp. 217-231, 2011.

S. Grundmann, E.L. Sayles, C.J. Elkins and J.K. Eaton: Sensitivity of an asymmetric 3D diffuser to vortex-generator induced inlet condition perturbations. *Exp. in Fluids*, Vol 52, pp. 11-21, 2012.

S. Jakirlić and K. Hanjalić: A new approach to modelling near-wall turbulence energy and stress dissipation. *J. Fluid Mech.*, Vol. 439, pp. 139-166, 2002.

S. Jakirlić, G. Kadavelil, M. Kornhaas, M. Schäfer, D.C. Sternel and C. Tropea: Numerical and physical aspects in LES and hybrid LES/RANS of turbulent flow separation in a 3-D diffuser. *Int. J. Heat and Fluid Flow*, Vol. 31, pp. 820-832, 2010.

S. Jakirlić, G. Kadavelil, E. Sirbubalo, D. von Terzi, M. Breuer and D. Borello: 14th ERCOFTAC SIG15 Workshop on Turbulence Modelling: Turbulent Flow Separation in a 3-D Diffuser. "Sapienza" University of Rome, September 18, 2009, *ERCOFTAC Bulletin*, December Issue, No. 85, pp. 5-13, 2010

J. Kriegseis, C. Schwarz, C. Tropea and S. Grundmann: Velocity-information-based force-term estimation of dielectric barrier discharge plasma actuators. *Journal of Physics D: Applied Physics*,Vol. 46, pp. 055202, 2013.

I. Maden, R. Maduta, J. Kriegseis, S. Jakirlić, C. Schwarz, S. Grundmann and C. Tropea Experimcntal and Computational study of the flow induced by a plasma actuator. *Int. J. Heat and Fluid Flow*, Vol. 41, pp. 80-89, 2013.

R. Maduta and S. Jakirlić: An eddy-resolving Reynolds stress transport model for unsteady flow computations. In "Advances in Hybrid RANS-LES Modelling 4" *Notes on Numerical Fluid Mechanics and Multidisciplinary Design*, Vol. 117, S. Fu, W. Haase, S.-H. Peng and D. Schwamborn (Eds.), pp. 77-89, Springer Verlag, ISBN (978-3-642-31817-7)

F.R. Menter, Y. Egorov: The Scale-Adaptive Simulation Method for Unsteady Turbulent Flow Predictions. Part 1: Theory and Model Description. *Flow Turbulence and Combustion*, Vol. 85, pp. 113-138, 2010.

E. Moreau: Airflow Control by Non-Thermal Plasma Actuators. *Journal of Physics D: Applied Physics*, Vol. 40, pp. 605-636, 2007.

J. Ohlsson, P. Schlatter, P.F. Fischer, D.S. Henningson: Ditect numerical simulation of separated flow in a three-dimensional diffuser. *J. Fluid Mech.*, Vol. 650, pp. 307-318, 2010.